BEAM DIAGNOSTICS FOR THE FRONT END TEST STAND AT RAL

S. Jolly, D. Lee, J. Pozimski, P. Savage (Imperial College, London, UK)
D. Faircloth, C. Gabor (STFC/RAL, Chilton, Didcot, Oxon, UK)

Abstract

The Front End Test Stand (FETS) at the Rutherford Appleton Laboratory (RAL) is intended to demonstrate the production of a 60 mA, 2 ms, 50 pps chopped beam required for future high power proton accelerators. A number of different diagnostic systems are currently under development to provide precise measurements of the H^- ion beam produced by the FETS ion source. A pepperpot emittance measurement system, which is also capable of high resolution transverse beam density measurements, has been designed for use on the ion source development rig. This system is capable of sub-microsecond time-resolved measurements at a range of positions along the beam axis. Details are given of the current design, with recent emittance and beam profile measurements presented.

INTRODUCTION

As part of the ongoing development of future high power proton accelerators (HPPA's) and to contribute to the UK design effort on the neutrino factory, the Front End Test Stand (FETS) is being constructed at the Rutherford Appleton Laboratory (RAL) in the UK. The aim of FETS is to demonstrate the production of a 60 mA, 2 ms, 50 pps chopped beam; a detailed description of the project is given in [1]. To provide the necessary low emittance, high current H^- ion beam for FETS, an ion source development program is currently under way. The aim is to increase the extracted beam current from 35 mA to 70 mA and to increase the pulse length from 250 μs to 2 ms over the current ISIS H^- ion source at RAL, with an *rms* emittance of 0.3 π mm mrad (for more details of the ion source, see [2]).

As part of the development program, and to provide necessary information for FETS beam dynamics simulations, high quality correlated emittance and beam profile measurements are required [3]. Two types of beam profile and emittance measurement are being developed, based on photo detachment by laser. These will provide non-invasive measurements of both the longitudinal and transverse profile of the beam: more details are given in [4]. In addition, a pepperpot device has been developed to provide correlated 4-D emittance measurements. Previous measurements made with a slit-slit emittance scanner had a number of shortcomings: 1) measurements in the horizontal and vertical planes must be made independently, with no information on x-y correlation or 2-D beam profile; 2) the distance (z) from the ion source extraction was too large and fixed leading to a very large beam diameter; and 3) the slit length is too small, rejecting the outer part of the beam and resulting in an artificially low emittance measurement.

THE FETS PEPPERPOT

The purpose of the FETS pepperpot emittance measurement system is to provide correlated 4-D emittance information and high resolution beam profile measurements at a range of positions along the beam axis of the ion source. The current Mk.II FETS pepperpot is a significant improvement over the previous Mk.I system described in [3]. The principle is identical: an intercepting screen splits the beam into beamlets, which are allowed to drift and are imaged by a scintillator screen; however, many parts of the current system are significant upgrades.

Mechanical Assembly

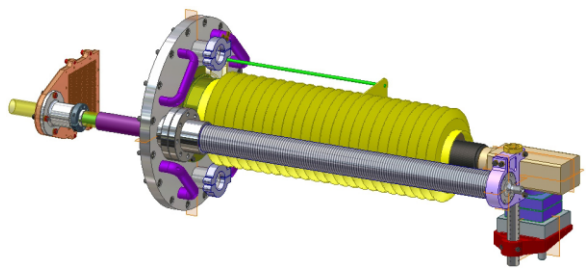

Figure 1: 3-D model of the pepperpot assembly; intercepting head is at the far left, camera and support is on the right.

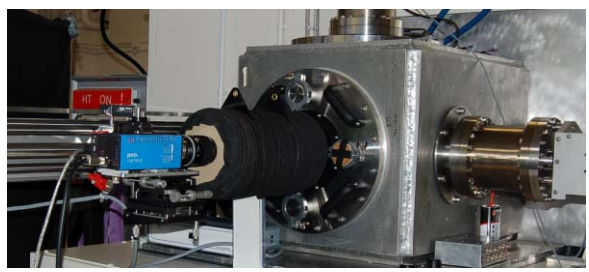

Figure 2: The FETS pepperpot, mounted to the ion source development rig. The existing emittance scanners are mounted to the top and right of the tank.

A 3-D model of the Mk.II pepperpot assembly is shown in Fig. 1. The pepperpot assembly consists of 3 main elements: an intercepting head, a high speed CCD camera and a main support structure. The head consists of a tungsten intercepting screen sandwiched between two copper plates. The intercepting screen is a 100 μm thick tungsten foil with a square array of 41×41 holes, each 50 μm in diameter, on a 3 mm pitch [5], giving a total imaging area of 120×120 mm^2. Laser drilling produces tolerances of less

than 10 μm in both hole size and absolute position. The front and back support plates are copper with an identical hole array to the intercepting screen, but with 2 mm diameter holes, and are 2 mm and 10 mm thick respectively. The front plate absorbs a significant fraction of the incident beam and the back plate provides the 10 mm drift length and prevents the beamlets from overlapping; both provide improved cooling to the tungsten screen. Mounted to the back of the rear copper plate is a single $152\times152\times6.4$ mm pure quartz scintillator plate. A second, interchangeable head is also used for high-resolution profile measurements: mounted into a copper frame, the entire surface of the quartz plate intercepts the beam, without the tungsten mesh and copper support plates.

The scintillation light from the quartz plate is imaged with a PCO 2000 high speed camera with a 2048×2048 pixel, 14-bit monochrome sensor and a Nikon 105 mm f/2.8 macro-lens; this interfaces with a PC via a high-speed Firewire connection. The camera is mounted on a system of Newport linear and tip-tilt stages that provide full 6-D position adjustment . The camera-to-screen distance is currently fixed at 1100 mm providing a resolution of 70 μm per pixel and an angular resolution of 7 mrad. The entire camera and head assemblies are mounted at either end of a linear shift mechanism, with a 700 mm stroke, mounted on a CF64 flange with a CF35 travelling flange. 38 mm bore stainless steel edge-welded bellows with an internal support tube keep the head and travelling assembly under permanent vacuum. A side mounted DC motor and controller with a linear digital vernier provide precise control over the longitudinal position of the assembly.

The central support rod passes through a rotatable CF64 flange of a 400 mm stainless steel vacuum flange, which is mounted to the rear of the ion source development rig vacuum tank and is shown in Fig. 2 (*cf.* Fig. 2 in [2]). A central 160 mm ISO-K observation window allows the camera to view the scintillator screen. A neoprene-coated nylon camera bellow, 200 mm in diameter and mounted between the observation window and the camera lens, ensures the light path to the camera remains light tight. Three additional KF40 ports on the main vacuum flange allow illumination of the copper head with an external light source and provide access for additional instruments. Cooling of the pepperpot head is provided by a cold finger that passes through the main flange via the inside of the travel mechanism bellows. Two concentric stainless steel tubes allow water to pass down the central volume and back through the outer volume. The head is clamped to the cold finger and is cooled by conduction.

Calibration

During data taking, accurate calibration data is crucial in converting the pepperpot images into emittance data. 3 pieces of information are needed for calibration: the centre of the pepperpot mesh, the relative rotation of the tungsten mesh with respect to the camera, and the spot-to-spot spacing, in pixels, of the mesh. This information is obtained from 4 lines, forming a $9\,\text{mm}\times9\,\text{mm}$ square around the central hole, marked on the surface of the rear copper plate facing the camera. The 4 corners of this square provide all the necessary calibration information, allowing the position of each hole in the tungsten mesh to be precisely reconstructed within the data analysis software.

Data Analysis Procedure

Data is recorded from the camera direct to a multi-image TIFF file and analysed with Matlab. Emittance data is derived from the x' and y' angles from the beam axis of each beamlet produced by the pepperpot plate. This is calculated by measuring the difference between the position of the light spot produced by the beamlet on the scintillator (see Fig. 3a) and the predicted position of a beamlet with zero divergence *ie.* parallel to the beam axis. The predicted hole positions are generated from the calibration data and compared to the data image. The weighted centre of each light spot is used to calculate a rough emittance distribution; real emittance values are produced by calculating x' and y' values for every single pixel with an intensity above a cut threshold. Summing up the total pixel intensity for each spot provides the beam intensity information.

RESULTS

To illustrate the performance of the device, 2 sets of data were recorded using the pepperpot setup: 1) variation in z-position of the pepperpot head, from 0 mm to 300 mm in 100 mm steps, for constant extract voltage (13 kV) and beam current (34 mA); and 2) ion source extract voltages of 6 kV, 9 kV, 13 kV and 17 kV at a constant z-position of 0 mm. The position of the pepperpot head was measured some 57 mm downstream of the ion source exit plane; 300 mm is therefore approximately the same z-position as the slit-slit scanners. For all measurements the platform voltage (and therefore the beam energy) was held constant at 35 kV.

Results for a single measurement are shown in Fig. 3: the raw spot image in Fig. 3a is used to reconstruct both the intensity profile shown in Fig. 3b and the emittance. Quiver plots for dataset 1 are shown in Fig. 4: arrows indicate the mean beam divergence for each spot, overlaid with contours of beam intensity. The behaviour of the beam is broadly as one would expect, with a steady expansion in beam size along the beam axis; the corresponding emittance (indicated by the arrows) shows no obvious nonlinearities. The measured beam properties are summarised in Table 1. The steady increase in emittance for increasing z-position may indicate space charge effects: the level of space charge compensation will be investigated with future simulations. The flat top and bottom of the beam profile are the likely result of unwanted collimation occurring upstream of the ion source exit. Variation in extract voltage (Fig. 5) shows a distinct change in beam shape, density distribution and emittance. The change in beam shape

and emittance may be partly a result of the upstream collimation; however, other factors will also contribute. The change in extract potential will cause a change in the shape of the field within the extract region, and affect the shape of the discharge plasma. An increase in extract potential also requires a corresponding increase in the 90° sector magnet current, changing not only the bending field but also the focussing effect of the fringe fields. In addition, an increase in extract potential requires a corresponding decrease in the post-acceleration voltage to keep the total acceleration potential constant at 35 kV: transverse focussing from the fringe fields within the post-acceleration gap will change accordingly.

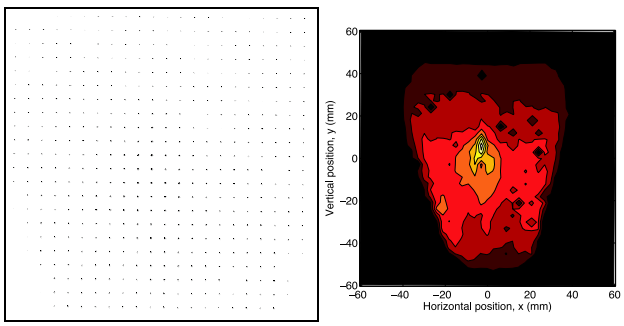

(a) Raw image (b) Beam profile

Figure 3: Enhanced section ($60\times60\,\mathrm{mm}^2$) of a raw data image, and the extracted 2-D density distribution, at 300 mm with 13 kV extract (*cf.* Fig. 4d).

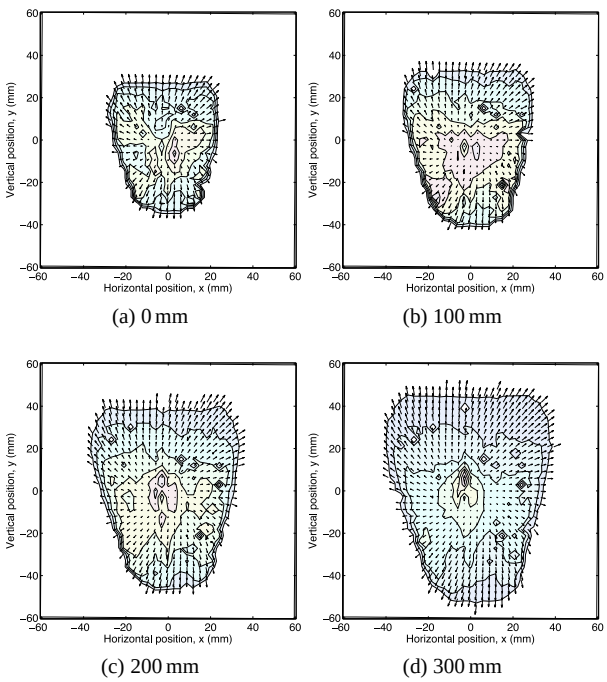

(a) 0 mm (b) 100 mm

(c) 200 mm (d) 300 mm

Figure 4: Variation in z-position with 13 kV extract.

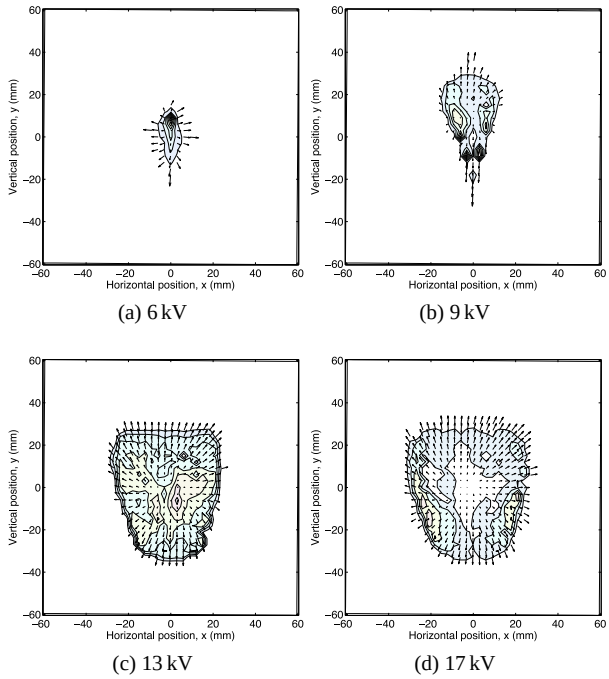

(a) 6 kV (b) 9 kV

(c) 13 kV (d) 17 kV

Figure 5: Variation in extract voltage at 0 mm: (a) shows strong asymmetric divergence in both planes; (b) shows mostly vertical expansion; (c) is nearly symmetric and slightly collimated and (d) is highly collimated.

Extract (kV)	Z (mm)	Beam size		ϵ (π mm mrad)	
		x (mm)	y (mm)	$\epsilon_{x,rms}$	$\epsilon_{y,rms}$
±1	±0.1	±3		$\pm5\,\%$	
6	0	18	33	0.25	0.77
9	0	27	63	0.74	1.14
13	0	51	60	1.36	1.47
13	100	57	72	1.65	1.78
13	200	69	87	1.82	1.96
13	300	78	102	1.90	2.04
17	0	57	63	2.02	1.92

Table 1: Beam properties for pepperpot measurements.

CONCLUSIONS

The advantage of the pepperpot method in the measurement of correlated emittance data has been clearly demonstrated. More detailed measurements are required to investigate the effects detailed above and to provide input data for beam dynamics simulations.

REFERENCES

[1] A.P. Letchford *et al.*, MOPCH112, EPAC 2006, p. 303.

[2] J.W.G. Thomason *et al.*, TUPLT141, EPAC 2004, p. 1458.

[3] S. Jolly *et al.*, TUPLS090, EPAC 2006, p. 1714.

[4] D. Lee *et al.*, TUPB11, these proceedings.

[5] Laser- und Medizin-Technologie GmbH, Berlin.